Analytica Chimica Acta 1107 (2020) 213–224

Contents lists available at ScienceDirect

Analytica Chimica Acta

journal homepage: www.elsevier.com/locate/aca

Construction of eco-biosensor and its potential application for highly selective, sensitive and fast detection of viscumin

S. Nasirahmadi [a], B. Akbari-Adergani [a], Sh Shoeibi [b, *]

[a] Nanotechnology Products Laboratory, Food and Drug Laboratory Research Center, Food and Drug Organization, Ministry of Health and Medical Education, P.O. Box 11136-15911, Tehran, Iran
[b] Food and Drug Laboratory Research Center, Food and Drug Organization, Ministry of Health and Medical Education, P.O. Box 11136-15911, Tehran, Iran

HIGHLIGHTS

- Selective detection of anticancer adjuvant called Viscumin was achieved.
- Surface molecularly imprinted polymer technology was used successfully.
- Co-administration of micro-contact and epitope approach was applied.
- The designed biosensor could successfully detect viscumin in complex matrices.
- First report on viscumin detection is declared by designed MIP-based biosensor.

GRAPHICAL ABSTRACT

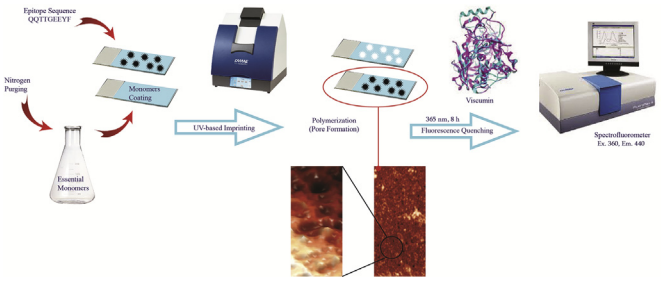

ARTICLE INFO

Article history:
Received 11 January 2020
Received in revised form
15 February 2020
Accepted 17 February 2020
Available online 20 February 2020

Keywords:
Nano-biosensor
Micro-contact
Imprinted polymers
Viscumin
Epitope approach

ABSTRACT

Viscum album lectin 1 (Viscumin) is one of the most important plant-based protein of potential adjuvant in cancer treatment. Therefore, the use of nano-biosensor technology as a novel emerges of biosensors is crucial to detect this modal agent in pharmacological study. Molecular imprinted polymer using 9-mer peptides sequence (epitope) was applied as a template. Using ultraviolet light, hydrogen bonding attained between the functional monomer and epitope, leading to the formation of a molecularly imprinted polymer. In the following, the epitope was derived from the surface of the polymer by sodium dodecyl sulfate (SDS) 2.5% and acetic acid 0.6% w/w. Finally, the designed nano-biosensor was exposed to different concentrations of the epitope. The selectivity of the nano-biosensor was tested in complex matrices such as blood plasma and urine. The scatchard analysis was covered for a consequence of the dissociation constants and the numbers of binding sites. Based on the results, the designed nano-biosensor has a limit of detection of 0.117 ng/μl and limit of quantification of 0.517 ng/μl in PBS buffer, respectively. These amounts stood 0.5 ng/μl and 0.8 ng/μl for urine environment and 1.25 ng/μl and 5 ng/μl for human blood fresh frozen plasma in the presence of ricin as the most homologue of viscumin (ML1) in fixed concentration (12:1), respectively. The time of detection and optimum pH was 8.0 min and 7.4, respectively. Designed and synthesized nano-biosensor is adequately qualified to be used in diverse complex areas, due to good efficiency.

* Corresponding author.
E-mail address: sh.shoeibi@fda.gov.ir (S. Shoeibi).

https://doi.org/10.1016/j.aca.2020.02.035
0003-2670/

1. Introduction

Every year, many types of cancers cause millions of deaths around the world, but many have not yet been cured effectively. So far, several methods have been developed to cope with cancer that has its own advantages and disadvantages. One of these proposed methods is the point of plant-based immune-toxins [1–3] as adjuvant along with other methods. Therefore, the timely identification of cancer treatment and its control is essential and important. Ribosome-inactivating proteins (RIPs) take place with a category of compounds distinguished in bacteria, plants, algae, and fungi. They display rRNA N-β-glycosidase action, which prompts to the cleavage of an adenine buildup at a conserved site of the 28S rRNA [4]. RIPs can be categorized into three types, discernible in type I, type II and Type III. The main important one is type II which made by a chain that shows the lethal rRNA N-glycosidase action (A-chain) and a lectin chain (B chain) as binding agents in the cell layer receptor. Emphasized toxicity level of type II RIPs compared with type I RIPs is because of its recognizable character, interceded by A-chains. The lack of the "A" chain essentially confines the entrance of type I RIPs into cells, approving its cytotoxicity minority. Diverse reports have highlighted the presence of a nearby connection among RIPs cytotoxicity and intracellular directing, which may change between various cell types relying upon: (A) expression of different types of restricting particles on cell surface [5,6], (B) sorting of RIP-ligand edifices to various compartments [7,8] and (C) existing of different pathways for the translocation of the toxic protein into the cytosolic chamber [9–11].

These contemplations are additionally substantiated by the presence of non-lethal RIPs, recognized in a few plants, that in spite of having N-glycosidase action are non-poisonous, since they are debased as an aftereffect of an intracellular directing unique in relation to that of harmful type II RIPs [12,13]. All in all, Type II RIPs (e.g. Viscumin, Abrin, Ricin, …), diffuse by means of endocytosis, since connection to galactose portions, and conveyed from Golgi system to the endoplasmic reticulum (ER) by retrograde vesicular transport. Consequently, in the ER receptacle, the A (dynamic) and B (binding) chains are separated; lastly the dynamic chain is conducted to the cytoplasm of host target [7–9]. Type III RIPs contain an amino-terminal area look like to type I RIPs and a carboxyl terminal space with obscure capacity, including grain JIP60 and maize ribosome inactivating protein b32 [14,15]. This type of RIPs is considerably less common than the other two types. Actuation of type III RIPs requires the expulsion of carboxyl end limit.

Discovery and observing of previously mentioned high-risk biological agents is so essential keeping in mind the end goal to create social insurance, healthcare issues, and security improvement. Nevertheless, pertinent discovery apparatuses and methods are tedious and work escalated. Some researchers have pointed to the role of small molecule-based pellets in the biomedical sciences [16]. The role of biosensors today for therapeutic purposes such as cancer is undeniable [17]. Also, some potential platforms are introduced in bio-sensing concepts, too. Although scientifically these platforms are valuable and improved bio-sensing concepts, but are usually complicated and suggested to be compromised based on parameters such as economic issues, simplicity and ease of use to be applied in routine bio-sensing assays [18,19].

Adapting to such an issue particularly in crisis and emergency mode persuade us to choose another better devices named nano-biosensors for fast detection. Typically, systematic strategies request both specific and delicate perception of the desirable target. Normal antibodies, receptors or proteins have been used to meet these prerequisites. Since, they are biomolecules; their utilization is restricted to gentle conditions. Moreover, functionalization is requesting and prompts to cover problems on particular surfaces as transducers. In addition, they are by and large at a high cost or tedious to manufacture. The need to go around these impediments simulated (synthetic) receptors have been created and reported by other researchers [20–22]. Molecular imprinting, which was set up in 1972, is one way to synthesize such manufactured receptors [23]. Molecularly Imprinted Polymer (MIP) relying on micro-contact approach is a powerful technique being ready to copy their natural rivals, for example, antibodies and natural receptors, helpful and remedial to independent and dissect convoluted samples as well, organic and ecological examples leading to resolve a few problems as a serious challenge in supramolecule fast detection. Consequently, micro-contact imprinting technique allows getting closer to overcome the aforementioned drawback as well as reaching low-cost, selective, highly sensitive, and suitable recognition platform useful for e.g. bio-sensing concepts. There are limited reports on development of not only nano-biosensors but also even biosensors for early diagnosis of similar RIPs proteins [24].

To the best of our knowledge, until now, there is not such a nano-biosensor based on MIP for detection of viscumin, a plant–based protein toxin in mistletoe. Also, there is not such a developed nano-biosensor by co-administration of epitope sequence and micro-contact approach upon plant-based toxin (viscumin …), too. The general objective of the research was to detect viscumin based on MIP-based biosensor in laboratory scale. The specific objectives of the study were to introduce epitope approach as well as micro-contact to assess its effectiveness for protein detection in order to knock out parts of macromolecules imprinting challenges.

2. Materials and methods

2.1. Chemicals and reagents

All standards and samples were prepared using 18 MΩ cm^{-1} deionized water (Millipore, Le montsur-Lausanne, Switzerland). All solvents were HPLC grade and obtained from Merck (Darmstadt, Germany). 9-mer peptides (95% purity) designed bioinformatically and synthesized by Biomatik Company (Peptide Synthesis Service, Canada). The peptide stock solution was prepared in buffer (PBS) at a concentration of 1000 μg/mL and stored at 4 °C until analysis. All buffers were established with water processed using a reverse osmosis step with a Milli-Q system from Millipore (Bedford, MA, USA). Prior to use, all buffers were filtered through a Millipore filter (pore size 0.22 mm) and degassed for 1.0 h. The working standard solutions in different concentrations (0.05–100 μg/l) were obtained by diluting appropriate amount of stock solution with aforementioned deionized water. Ethylene glycol dimethacrylate (EGDMA) and 2, 2′-azobis isobutyronitrile (AIBN) from Sigma–Aldrich (Steinheim, Germany) were of reagent grade and were used without any further purification. Methacrylic acid (MAA) from Merck (Darmstadt, Germany) was distilled in vacuum before use to remove the stabilizers. All other chemicals used were of analytical grade.

2.2. Preparation of the micro-contact-epitope (ML1) imprinted glass

The micro-contact-epitope imprinted glasses were prepared in three steps:

(a) Preparation of the glass cover slips (protein stamps): Glass cover slips (24*40 mm) were used for the preparation of protein stamps in this procedure. In the first step, cover slips were cleaned in 20 mL of 1.0 M HCl, de-ionized water, 1.0 M NaOH, deionized water and ethanol, respectively in an

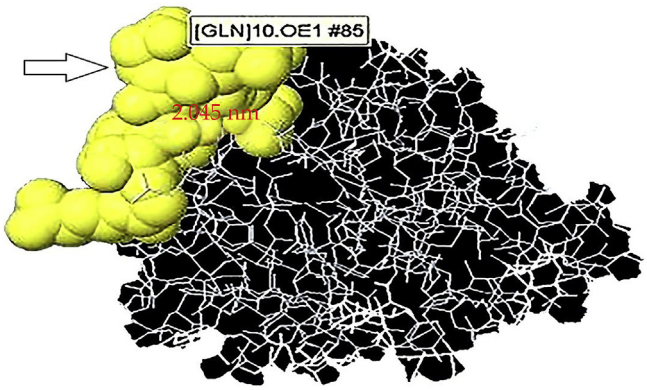

Fig. 1. Steric position of selected epitope (9-mer peptide) obtained with average horizontal width of 2 nm using online Cn3D software (depicted with white arrow) and bioinformatics studies based on epitope approach.

ultrasonic cleaner for 5.0 min in each step. After cleaning, the cover slips were dried with nitrogen gas.

(b) The cleaned cover slips were immersed in piranha solution (H_2SO_4: H_2O_2) in ratio of 3:1 and then in (10% (v/v) APTES (3-amino-propyl-triethoxysilane) in ethanol at 55 ^{0}c for 90 min to introduce amino groups on the surface. Subsequently, the glasses were rinsed with ethanol to remove any unbound APTES molecules. In the last step, suitable amount of peptides was coated on the surface of cleaned up glass by the mechanism of surface adsorption (30 min). Finally, the cover slips were washed with phosphate buffer (1X) and then, dried with nitrogen gas. They were kept at 4 °C in a closed petri dish until use.

(c) Micro-contact imprinting of 9-mer peptides as an indicator epitope of viscumin (ML1) onto the pretreated glass: The monomer solution containing MAA (methacrylic acid) and EGDMA (ethylene glycol dimethacrylate) (1.0 mM: 1.5 mM) was prepared and Fluorescent dye as reporter and the initiator (AIBN) were added to this solution. Monomer solution (300 μL) was pipetted onto the glass surface. Then, the protein stamp (the glass cover slip) was brought into contact with this monomer solution which had the contact angle of 15^0. The polymerization was initiated under UV light (365 nm, 100W) and continued for 8.0 h. After polymerization, the cover slip was removed and any template peptide (epitope) that got stuck on the glass surface was eluted away. This elution/washing was done as a security step since the print peptide was immobilized on the glass plate and would in principle stay on that plate, thereafter be removed when the plate was taken away. When not in use, glass was kept at 4.0 °C in a closed petri dish filled with nitrogen gas. Non-imprinted (NIP) electrodes were prepared with the same procedure without immobilization of the template peptide, 9-mer epitope, onto the glass cover slips.

2.3. Apparatus

Spectrofluorometer (PerkinElmer LS 55) instrument was used for chromatographic analysis of epitope as an indicator of viscumin (ML1) in different complicated matrix. The PerkinElmer LS 55 Fluorescence Spectrometer offers flexibility, versatility, reliability and ease-of-use. The LS 55 spectrometer includes a host of automated accessories and software to deal with a wide range of bio research applications. The LS 55 is built on PerkinElmer's heritage of sensitivity and reliability. All of the analyses were carried out at 360 nm (excitation wavelength) and 440 nm (emission wavelength), respectively. In all solutions, the pH was adjusted by digital Metrohm pH meter (model 744) equipped with a combined glass–calomel electrode. The characterization of the nano-biosensor was performed by transmission FTIR (Fourier-transform infrared spectroscopy) spectroscopy in the mode of ATR (Attenuated total reflection) (Nexus470, Thermo Nicolet, USA), mercury porosimetry-an analytical technique used to determine various quantifiable aspects of a material's porous nature, such as pore diameter, total pore volume, surface area, and bulk and absolute densities-was employed to investigate the porosity of the nano-biosensor surface designed by the model gyroscope, the Pascal440, the Thermo Finnigan factory in Italy and AFM (Atomic Force Microscopy). FTIR spectra of optimized biosensors containing nano-pores were recorded on a Shimadzu FTIR 4300 spectrometer (Shimadzu, Kyoto, Japan) in the range of 400–4000 cm^{-1}. AFM (NT-MDT, Next, Russia) was employed to determine the shape, size histogram and surface topography of the photo-grafted glass as nano-biosensor surface. The rate of absorption of standard epitope solutions as well as preparation of appropriate dilutions from epitope was achieved by utilizing UV/Vis, two-beam spectrophotometer CE7250, the construction of the Cecil factory in the United Kingdom.

2.4. Buffer preparation

To prepare the phosphate buffer, at pH = 7.4, at first, disodium hydrogen phosphate (1.44 g), sodium dihydrogen phosphate (0.25 g), sodium chloride (8.0 g) and potassium chloride (440 g) weighed and then dispersed in distilled water balloon following by dispensing in a volume of 1000 L.

2.5. Preparation of standard epitope solution

To prepare the standard epitope solution, phosphate buffer saline (pH = 7.4), was used. The standard epitope solution was tested in the concentration range of 0.5% ng/μl to 100 ng/μl prepared from 1000 ng/μl stock solution. Then, the calibration curve was prepared by drawing the absorbance of the epitope at the wavelength of 280 nm applying spectrophotometer.

2.6. Bioinformatics studies

Considering that the purpose of the paper was the design of the MP-based nano-biosensor, regarding that in this type of sensor, the biological agent should be used as a probe to detect biological agent (ML1). Therefore, for the purpose of the above-mentioned goal, bioinformatics study was conducted to reveal and predict the specific linear B-cell epitope. First, a sequence of 4 types of ribosome inactivating proteins (RIPs) toxins of type AB was extracted and examined. The sequences were adapted in the FASTA format extracted from the protein data bank. Then, multiple sequence alignment was run to compare their sequences and examine their unique points in order to find an epitope candidate. After analyzing and comparing the different parts of the nine-segment c-terminal peptide sequences from the catalyst toxin (viscumin) chain with the least possible interference, QQTTGEEYF was selected for further investigation. For further and more detailed studies, the isoforms sequences in the data banks of this toxin were examined and multiple alignments carried out to determine the conserved domain of the selected peptide. By comparison, it was found that the candidate comprised a good conserved domain in different isoforms of favorite toxin. For further investigation, the sequence of the chain (A) of the toxin in different data banks was searched with

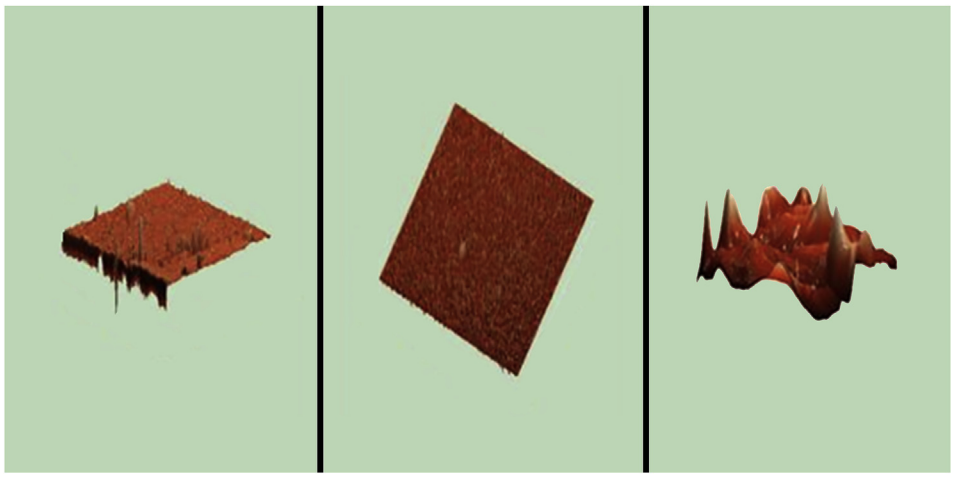

Fig. 2. Different steps of glass slide (sensor backbone) treatment from left to right: after surface clean up (A), after modification with piranha solution (B) and following silanization step (C).

different tools, using the first structure of the protein through the online network software, like as Cbtope and other similar databases. The possibility of the presence of the selected peptide applying as an epitope approach in the viscumin protein toxin sequence was investigated. The results indicated that in all cases, whole part of this peptide or a large portion of it is predicted to be as epitope with a precision of over 70% in most cases just applying mentioned limited online available software, and were the only option among other peptides. In all over online bioinformatics network, aforementioned peptide has been introduced as potential candidates for epitope. It is noteworthy to mention that the priority of applied design was based on synthetic biological element conservancy than epitopic aspect of 9-mer peptide (biological element) in toxin structure which is normal and acceptable criteria for detection issues in biosensors. Conservancy is a sufficient criterion due to the target of present work as to evaluate the reliability of epitope approach theory in viscumin detection in lab scale and not applying in field applications. It is also known that when a peptide fragment has a conservancy property, it means that it is certainly an important cornerstone of its protein structure origin and that it cannot be easily altered during its evolution years or at least undergo the slightest change in its biochemical structure (amino acid sequence). Although having the benefit of both aspects (conservancy and epitopic features) stand more powerful platform for detection issues leading to more sensitive detection, but designing epitope approach parameters is a limiting factor which make it difficult to achieve the benefit of both aspects. Consequently, the 9-mer QQTTGEEYF was suggested as a suitable candidate applying in epitope approach of MIP-based nanobiosensor for detection of ML1 (Fig. 1- by arrow in yellow).

2.7. Statistical analysis

All facts are presented in this text as mean result ± SD (standard deviation). Statistical analysis was assessed applying the *t*-test and considered significant at $P < 0.05$ level. All figures presented in this article have been received from 3 unbiased experiments with similar results.

3. Results and discussion

3.1. Characterization studies

3.1.1. Morphology and topography of MIPs

Fig. 2 (A, B and C) show the AFM images of bare surface after cleanup process, modified surface and functionalized surface of glass surface respectively. The uniformly sized nano-pores of MIPs were made onto the surface of glass when the nano-biosensor was contacted with the peptide solution. This performed through the arrangement of a few self-assembly complexes from MAA monomers which were stacked into the pores of the nano-biosensor. Conditions of monomer regarding high dilutions, suitable amount of template: functional monomer: cross-linker, in-situ polymerization and mellow condition amid the polymerization handling made such a smooth, nano-sized and consistently dissemination of synthesized nano-pores. After polymerization and evacuation of the layout molecules, various imprinted polymeric nano-pores were accomplished. In any case, it was watched that the altered surface was smooth and in great assenting with past modified plan. Besides, self-evident contrasts can be watched within the AFM pictures (Fig. 2). Uncovered surface after washing steps has changed peak structure (Fig. 2A), whereas noteworthy alter was watched in its morphology after adjustment with piranha solution in MIPs. Lower peaks in the AFM image (Fig. 2B) depicted that modification of the surface was successfully achieved. The effect of silanized agent on the morphology of the glass surface is also depicted (Fig. 2C). It was found that the silanization process carried out onto the surface of glasses successfully. However, size of the NIP larger than the MIP particles, approving the 9-mer peptides as good candidate in epitope (biological element) approach had significant influence on pore (imprinted site) formation during the in-situ (UV-based) polymerization. The imprinted polymer system formed in the presence of MAA approved as a proper functional monomer [25,26]. Within the nonattendance of epitope, MAA can form hydrogen reinforced dimers within the non-imprinted framework. The pre-polymerization solution contains both free MAA and MAA dimers. Within the imprinted framework, there's an extra molecular interaction between MAA and epitope candidate, which might somehow influence the development of the cross-linked polymer cores, so that it is anticipated to create smaller pores.

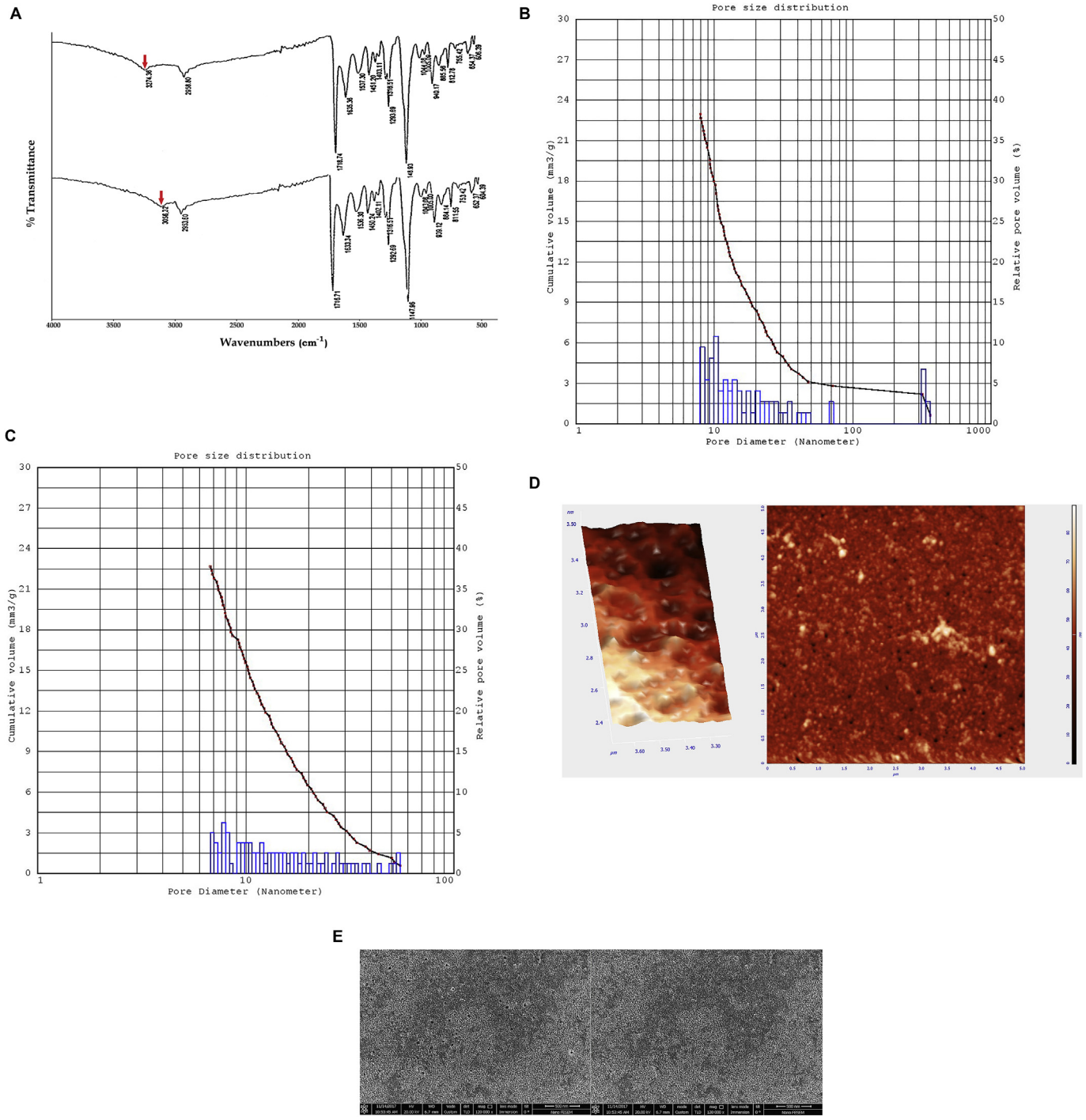

Fig. 3. (A) IR spectra of MIP in two mode: upper (with template) and lower (without template), Nano-pores characterization of MIP (B) and NIP (C) by mercury porosimetry, AFM (D) and FE-SEM (E) characterization tests of MIP (left) and NIP.

Table 1
Different molar ratios of epitope to functional monomer.

Polymer (nano-biosensor)	Ratio of Epitope/Functional monomer (mmol)	Emission (490 nm)
MIP_1	2: 1	3.8
MIP_2	4 : 1	5.6
MIP_3	6 : 1	3.7
MIP_4	8 : 1	1.8
MIP_5	10 : 1	1.5

Table 2
Nano-biosensor response in three moods of washed, rebounded and re-washed (Rejuvenation in nano-biosensor construction).

No.	Washed (mean ± SD)	Rebounded (mean ± SD)	Re-washed (mean ± SD)	RSD% (n = 3)
MIP 1	5.70	4.80	5.65	0.39
MIP 2	6.50	4.60	5.54	0.43
MIP 3	5.20	4.10	5.15	0.41

3.1.2. IR spectra, mercury porosimetry, morphology and size determination study

The IR absorption spectrum of the imprinted poly (MAA-co-EGDMA) UV-aided complex in nano-biosensor is shown in Fig. 3A. The IR spectra of MIP before and after template removal displayed different characteristic peaks, indicating the success of removal step. The O–H stretching and the C=O stretching vibrations in the MIP (before template removal) are seen at 3056.32 and 1716.71 cm^{-1} while these peaks in the MIP (after template removal) are seen at 3274.36 and 1718.71 cm^{-1}, respectively. This displacement toward lower frequencies is due to the hydrogen bonding of the O–H and the C=O groups of MAA with amine groups in epitope in the undiluted template MIP. Other absorption peak that observed in both modes is relatively wide band at 2958.80 cm^{-1} for stretching of aliphatic C–H bond. There were also other differences between IR spectra of the removed and non-removed template of MIPs in stretching vibration of residual vinyl C=C bonds. In the unremoved polymer, there was one sharp band with low relative intensity at 1635.36 cm^{-1} that appeared at 1633.34 cm^{-1} in the corresponding removed template of MIP. Additional absorption peaks match both those of MIP in two modes. The shifts of further peaks in each of the two modes match carefully. Mercury porosimetry is another method for studying porosity of materials, such as porosity size, porosity volume at the surface, the material volume and the absolute density of matter. With the help of this method, not only porosity but also pore distribution fields can also be specified. The basis for measuring porosity with this method is that of mercury with high pressure, it enters the porosities sampled and measures the amount of pressure required to counteract surface tension, the amount of porosity can be calculated from the fluid and its entry into the porosity [27]. Occupied volume of present nano-biosensor is depicted in Fig. 3B and C which are regarded as MIP and NIP, respectively. Based on the obtained results, more than 90% of the imprinted sites are in the nanometer ranges (1–100 nm). This range of sizes is due to the controlled synthesis of thin film as well as the applied micro-contact technique which leads to better sensitivity and a lower limit of detection time. On the other hand, to reveal the morphology and approve the size of imprinted sites as nano-pores, AFM and FE-SEM characterization tests were carried out. As it can be deduced (Fig. 3D and E), both of them approved the formation of nano-pores with globular morphology in the polymer matrix onto the surface of nano-biosensor.

3.2. Optimization of formulation in MIP-based nano-biosensor

There are numerous variables, including quantity of functional monomer or structure of cross-linker as nature and porogen that impact the very last mechanical and adsorption traits of the acquired MIP in terms of affinity, capacity and selectivity for the viscumin. The primary experiments upon the applied 9-mer epitope candidate revealed that the imprinted polymers prepared in buffer (phosphate buffer, pH = 7.4) show relatively good molecular recognition ability in aqueous extraction media obtained well controlled physical forms for the molecular film and its nano-pores. Due to the structure of the epitope (viscumin) owning primary amino anchors which make it a flawless compound to have interaction with methacrylic acid monomers in the polar solvent. Accordingly, the use of those monomers results added recognition capacity to desired analyte by definite interactions with the template in the relevant porogen. This feature may achieve due to the high rate of tolerance originated from acquired cross-linker. For this reason, specific formulation for the obtainment of optimized MIPs with stepped forward molecular recognition competencies were used in the previously aforementioned buffer (pH = 7.4, 0.01 M) (Table 1). Obtaining valid molar ratios of functional monomer to template are very critical to decorate unique affinity and quantity of MIPs recognition sites within the nano-biosensor. Unregulated ratios of functional monomer to template result in excessive non-specific affinity, even as low ratios produce complexions because of insufficient functional moieties [28]. The pre-polymerization solution was prepared with different crosslinking ratios to the antibody and nano-biosensors were made with this solution. Nano-biosensors with different ratios were exposed to a 10 ng/μl concentrations of antibody solution and after washing, the amount of emission release (without analyte) wavelength was studied with a fluorescence spectrophotometer at 490 nm and the obtained data was compiled (Table 1). As showed in Table 1, the results of peptide uptake are increased by increasing the ratio of 1:2 to 1:4 (epitope:functional monomer) due to increase in functional groups and consequently formation of more bonding sites; hence, bonding efficiency is increased. This ratio had the best specific affinity and the highest recovery of 95% while that of the corresponding NIPs was low at 25% (data not shown). With increasing ratio to1:6, due to the formation of a non-specific binding site in the polymer network, the target analyte absorption rate is reduced. Therefore, the ratio of 1:4 with the highest loading of target analysis in MIP2 was optimum ratio in this study. Therefore, the typical 1:4 template/monomer molar ratio was used for further studies (MIP2, Table 1).

3.3. The performance of the sensor in terms of fluorescence or quenching

Three samples of MIPs made in the previous step in three separate washing, rebinding, and re-washed conditions at a non-optimal time and non-optimal solvent ratio (Table 2).

As seen from Table 2, in the washed state, the sensor values are higher than the rebounded state, and these results indicate that the sensor mechanism is based on quenching. In addition, with a simple comparison based on Table 2 and Fig. 2, it may be found that the removal solution had sufficient strength to remove the template.

3.4. Adsorption efficiency, desorption recovery, pH and optimum time of detection

Fig. 4 (A) shows the percentage of absorption efficiency of the nano-biosensor built versus time. As time increases, the amount of absorption increases. It then reaches its maximum at 8 min. After this time, the adsorption rate remains constant, indicating the saturation of the polymer binding sites of the molecular imprinted polymer at this time. Of course, this assay has been performed

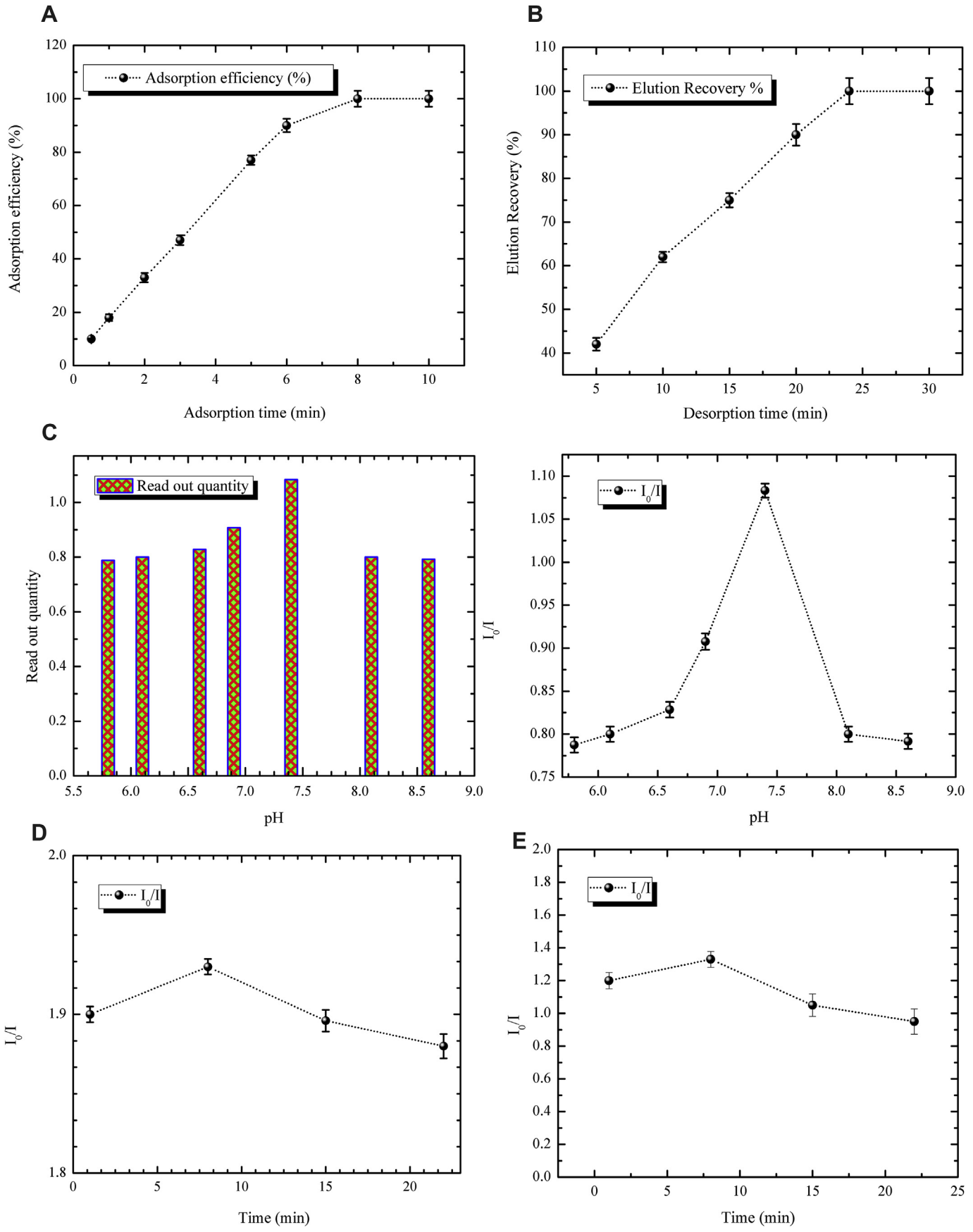

Fig. 4. Adsorption efficiency (A) and Desorption recovery (B) of nano-biosensor in preliminary synthesizing step, Effect of pH on quenching behavior of nano-biosensor (C_1 and C_2), Optimum absorption time in both MIP (D) and NIP (E).

Table 3
Effect of different pH on nano-biosensor quenching.

pH	I_o/I (mean ± SD)	RSD%
5.8	0.78	0.16
6.1	0.80	0.15
6.6	0.82	0.13
6.9	0.90	0.06
7.4	1.08	0.05
8.1	0.80	0.15
8.6	0.79	0.16

under the initial conditions of work without setting optimal conditions. Further, after optimizing some of the parameters, this time may increase or decrease. Fig. 4 (B) shows the percent recovery rate of nano-biosensors built against time. As time increases, recovery will increase. Finally, it takes 24 min to attain its maximum removal (recovery %) with optimized washing solution (SDS) 2.5% and acetic acid 0.6% w/w. After this period, the recovery rate keeps constant, indicating the almost complete loss of molecular template polymer bonded sites at this time. Therefore, the best time dedicated to clear binding sites with the highest recovery rate was 24 min. To explore the impact of nano-biosensor performance in the optimized pH, dissolved epitope with a settled concentration of 10 ng/μl at different pH (5.8, 6.1, 6.6, 6.9, 7.4, 8.1, and 8.6) was prepared. The sensor was immersed in a solution with definite content of protein and in this way, fluorescence power was measured at various pH, then after fluorescence intensity was plotted versus applied pH. As appeared in Fig. 4C_1 and C_2 (Table 3), the optimum pH for distinguishing the best working condition of epitope was achieved at pH = 7.4. At acidic pH, protonated amine groups of epitope will most likely be unable to interact with the polymer functional groups and henceforth will reduce the adsorption of the template. At acidic pH, the carboxyl groups of epitopes and functional monomers may separate and will have the ability to interact slowly. There are a couple of free electrons on atoms, for example, nitrogen, oxygen et cetera would prompt control of lower energy transmissions as *n-π in comparison with higher energy transmissions of * π-π. The transmissions of * n-π promptly reduce in fluorescence intensity, lead to the expansion in phosphorescence intensity. Clearly, transmissions of * π-π are in charge of fluorescence discharges in compounds containing double bonds. Further protonation of atoms prompt all the more obstructing of their free electron pair, thus transmissions of * n-π may not occur. As a consequence, transmissions of * π-π will command and prompt increment of fluorescence intensity. In this manner, the distinction in fluorescence extinguishing in acidic pH compared with a basic pH is credited to the higher rate of fluorescence intensity made by fluorescent monomer. To evaluate the optimal response time of a nano-biosensor, it was exposed to a solution comprised of target analyte and calculated rate of quenching at discrete time intervals (Fig. 4). At the initial time (1 min), there were more sites which have not been filled with analyte. Then, from 1.0 to 8.0 min, the amount of quenching increased and then the amount of changes was almost stable after 8 min. The aforementioned behavior in MIP was similar to NIP (control). The results show that after 8.0 min, the nano-biosensor specific binding sites are filled with analyte. Based on figures (4D, 4E), a maximum gradient with a steep slope is observable, which expresses the fast kinetic of designed nano-biosensors. Therefore, the optimal response time of the nano-biosensor was considered to be 8 min. Consequently, the duration of the contact time of MIP-based nano-biosensor with analyte of interest was considered in 8 min.

3.5. Scatchard analysis, stern-volmer plots, sensor response in PBS buffer and durability assay

A team of researchers conducted fluorescence biosensors based on the quenching mechanism, which yielded satisfactory results [35,36]. The binding properties of analyte in the present micro-contact-based (nano) biosensor are expressed by simple and reliable methods called scatchard analysis. As peptide displays the absorption at 280 nm, formation of the complex to peptide led to the enhancement of the intensity of the absorption with a slight red-shift (data not applicable). This result may suggest the presence of a static interaction in the complex due to the formation of a functional monomer epitope ground state system, which has been observed in other cases [29,30]. Herein, the fluorescent quenching may be attributed to static quenching. For static quenching interaction, the apparent binding constant (equilibrium constant) "K_b" and the number of binding sites "n" could be obtained from the fluorescence data according to the scatchard equation: $\log((I_0-I)/I) = \log K_b + n \log [Q]$ [31].

The binding isotherms were determined by adding a fixed amount of polymer to the various concentrations of epitope (0.05–20 ng/μl) (Fig. 5A and B). Distinguishing difference in binding properties between MIP and NIP was noted. However, scatchard plots presented in Fig. 5A revealed K_b and n of $0.046*10^3$ and 0.65 for MIP, and 10.76 and 0.2 for NIP, respectively. This result is characteristic of imprinted polymers obtained by the non-covalent approach. The binding constant of MIP compared to the NIP showed a difference quantity, indicating the selectivity of the sites created. Also, term of "n" quantity for related MIP is more than three orders of magnitude than control, i.e. NIP, so the synthesized MIP has more specific sites than control. The binding constant and the number of MIP and NIP sites based on scatchard plots are shown in Table 4.

All fluorescence quenching data were analyzed further by applying the stern-volmer (S–V) equations that examine different quenching mechanisms [32,33]:

$$F_0/F = 1 + Ksv [Q], \quad (1)$$

$$F_0/F = (1 + Ksv [Q]) \exp (V [Q]). \quad (2)$$

F_0 and F are the fluorescence emission intensities in the absence and presence of quencher. Ksv denotes the dynamic quenching constant, and V denotes the static quenching constant. The [Q] stands on the concentration of quencher. Equation (1) represents a linear function between dynamic quenching and quencher concentration, where quencher collision with the excited fluorophore returns it to the ground state without fluorescence emission [34]. Fig. 5C and D shows the linear S–V plots for epitope, which were best analyzed using (1). The Ksv for epitope in MIP is 0.0224 ($R^2 = 0.9771$). The Ksv for NIP (control) is 0.0078 ($R^2 = 0.9519$). Due to their suitable size, epitope could easily penetrate the porous structures of MIP specifically and NIP particles non-specifically. The optimal imprinting factor of the MIP sensor (i.e. IF) was 2.87. The expressed "IF" was originated from Ksv values that were in the different quantities. Consequently, it indicates proper selectivity of MIP compared to the NIP sensor. To establish the potential of nano-biosensor operation for the selective detection of analyte, the MIP/NIP films were applied to the detection of epitope in standard media (PBS buffer, 1X). Results from the quenching analyses and correlation between the epitope (representative of ML1) concentration and nano-biosensor response as I_0/I showed that the quenching calibration curve of epitope for PBS buffer solutions is linear in the ranges 0.05–20 ng/μl ($R^2 = 0.9965$). Recovery percent of the epitope with the MIP for buffer samples was 100%. The LOD

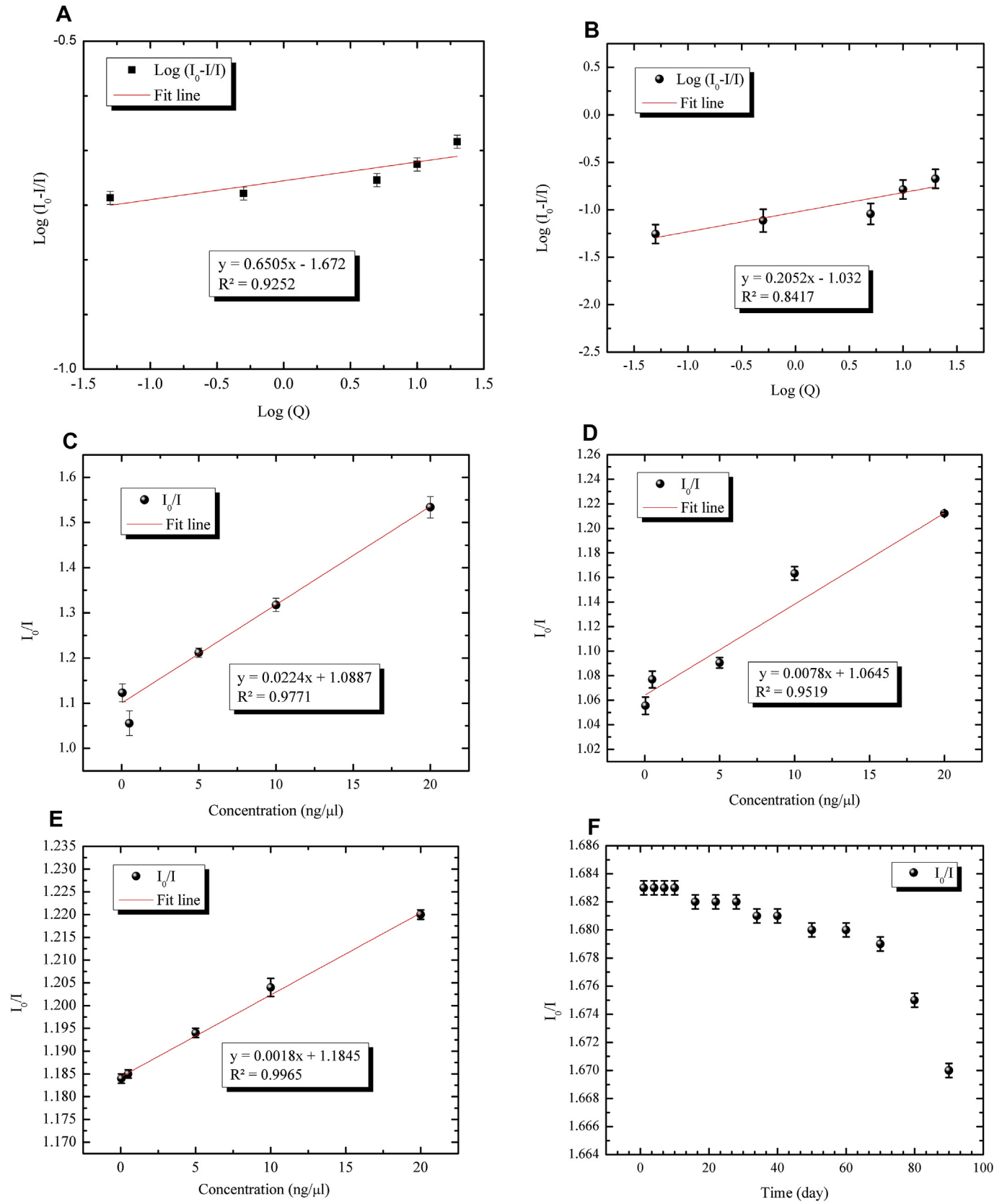

Fig. 5. Scatchard plots obtained for MIP (A) and NIP (B), Stern-volmer plot of MIP (C) and NIP (D), nano-biosensor response in PBS buffer as quenching curve (E) and Durability assay of nano-biosensor in blood plasma media (F).

Table 4
Parameters of scatchard plots.

Polymer	K_b [M^{-1}]	n	R^2
MIP	$0.046*10^3$	0.65	0.9252
NIP	10.76	0.2	0.8417

and LOQ for epitope in buffer samples were 0.173 and 0.577 ng/μl, respectively (Fig. 5E). The reproducibility and repeatability of the method were evaluated from run-to-run experiments (5.0 ng/μl epitope standard solution, n = 3) and different batch experiments (twelve batches) and RSDs of 3.2 and 4.38% for the detection run of epitope were obtained, respectively. For the examination on the durability of each MIP-based nano-biosensor, we measured the fluorescence quenching of output value of the sensor through a long period of time. After that, a real-time monitoring and detection of epitope were performed by nano-biosensor applying fluorescence spectroscopy technique to evaluate durability of the nano-biosensor in complex media. Due to some limitations, blood plasma was selected as the complex media of interest. The results of durability (recyclability) assay are shown in Fig. 5F. The fluorescence intensity in nano-biosensor was measured for the three times during a day. The quenching of the sensor was about stable until day of 80 (10% reduction) and then began to decrease more than 10%. Based on these results, the constructed nano-biosensor entailed acceptable durability for detection of conserved 9-mer peptide (viscumin representative) in the complex matrix (blood plasma). The constructed MIP-based sensor was recyclable i.e. at least 12 times (statistical data could be found in supplement data).

3.6. Nano-biosensor performance in complex media

It is clear that the true and ultimate function of a biosensor is a reliable one that can perform in repetitive and valid conditions in complex environments such as plasma and urine. Therefore, using this method, the concentration of 5 ng/μl of epitope in plasma and urine taken from one of the hospitals in Tehran (Iran) was exposed to sensors and its suitability records were recorded. Also, in order to test the performance of the sensor in the presence of a protein with a similar structure of viscumin with a concentration ratio of 20 to 1, sensors were exposed for 3 times. The average of the results was recorded. As the results show, the built-in nano-biosensor has been able to perform well in complex environments, even in the presence of twenty-fold concentration of analogous proteins, i.e. ricin (Fig. 6A, B and C). Recovery values in the mentioned environments were 97%, 107% and 99%, respectively. Therefore, according to the values obtained, as well as the defined recovery percentage for the sensor, i.e., 80–120%, in accordance with the international union of pure and applied chemistry, "IUPAC", standards definition stating that "specificity is considered to be the ultimate of selectivity; it means that no interferences are supposed to occur." In this regards, the term applies only to a method/sensor which is capable to exclusively detect the analyte, without suffering for any interference (100% selectivity) [37]. Referring to aforementioned definition, the performance of present nano-biosensor made for viscumin has excellent selectivity.

Molecularly imprinted polymer (MIP) for biological warfare agent (BWA) ricin was synthesized using silanes in order to avoid harsh environments at some stage in the synthesis of MIP by pradhan and co-workers [38]. The synthesized MIP was utilized for the recognition of ricin. The complete removal of ricin from polymer was confirmed by fluorescence spectrometer and SEM-EDAX. SEM image of Ricin-MIP exhibited nanopatterns and it was found to be entirely different from the SEM image of non-imprinted

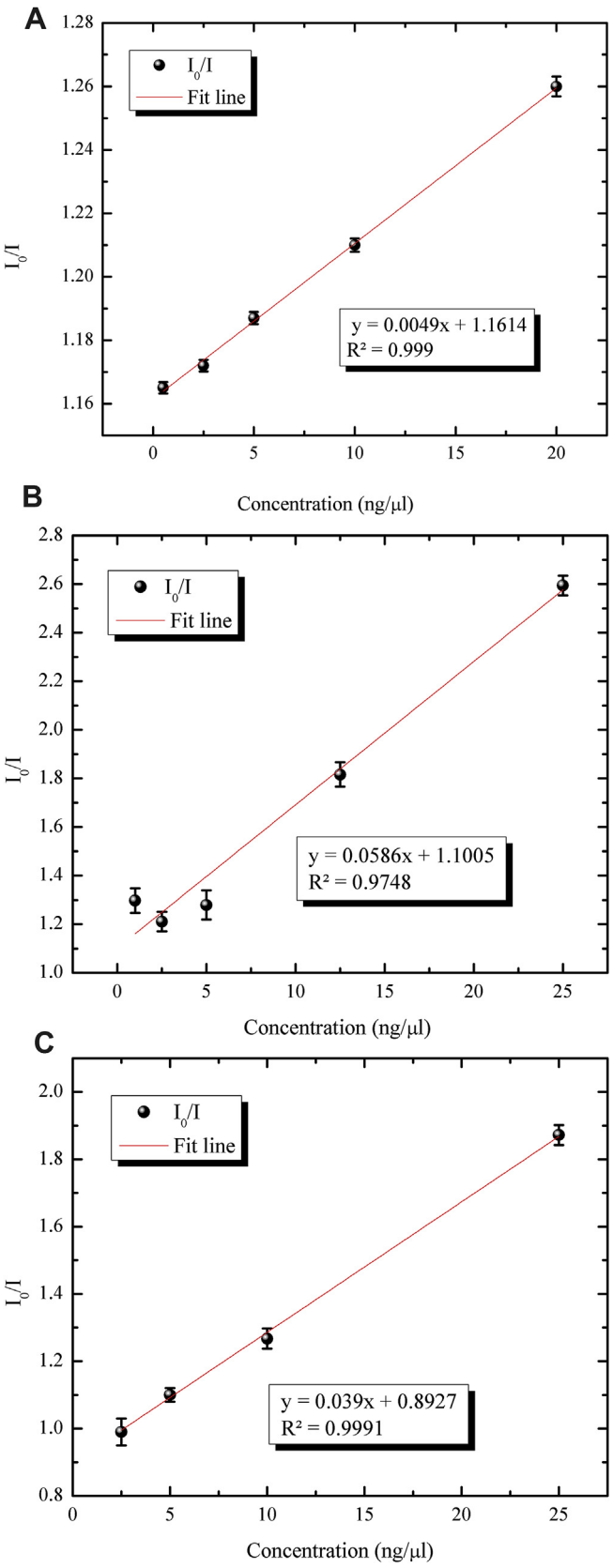

Fig. 6. Nano-biosensor performance in plasma (A), urine (B) and plasma media contain competitor protein so-called Ricin (C).

polymer (NIP). The same results inferred by present work using FE-SEM, AFM, simultaneously. BET surface area analysis revealed more surface area for Ricin-MIP than that of NIP. In addition, surface area study also showed more pore volume for Ricin-MIP than that of NIP confirming the presence of imprinted sites for ricin. In present work, the applied mercury porosimetry surface area analysis revealed the same results. In addition, surface area study also showed more pore volume for viscumin-MIP than that of NIP confirming the presence of imprinted sites for viscumin. The recognition and rebinding ability of the viscumin-MIP was tested in complex aqueous solution. Ricin-MIP rebound more ricin when compared to the NIP. Ricin-MIP exhibited an imprinting efficiency of 1.76 (the present work imprinting efficiency was close to 3) and it also showed 10% interference from the structurally similar protein abrin (our viscumin biosensor showed more than 90% recovery in the presence of similar protein ricin-slightly more than ricin-MIP reported sensor) [38]. In other works, Komarova and co-workers addressed the challenge of protein bio-sensing using MIP, and have developed as well as tested a novel approach to creating sensing conducive polymer films imprinted with a protein substrate, ricin toxin chain A (RTA). Their approach for creating MIP protein sensing films was based on a concept of substrate-guided dopant immobilization with subsequent conducting polymer film formation. In their work, three macromolecular dopants were tested with strong protein affinity. The films were formed using sequential interactions of the substrate, dopant and pyrrole, followed by electrochemical polymerization. The films were formed on gold array electrodes allowing for extensive data acquisition (our design was simpler using modified glass slides without complex design). The thickness of the films was optimized to allow for efficient substrate extraction, which was removed by a combination of protease and detergent treatment (complex design chosen by Komarova and co-workers). The MIP films were tested for substrate rebinding using electrochemical impedance spectroscopy (EIS). Out of three dopants tested, RTA-imprinted polypyrrole films doped with Coomassie BB performed with highest selectivity towards detection of RTA with a level of detection (LOD) of 0.1 ng mL (-1) [39]. Various fluorescent chemosensors were designed and produced by researchers to detect the cancer cells by detecting different ions related to aforementioned live cells in bio imaging application, too [40–42]. They have been successfully demonstrated and reported as good biomarkers. Hereafter, all of mentioned trend may be applied cooperatively for next generation sensors with more powerful abilities ib sensing concepts.

4. Conclusion

Molecular imprinting was applied to create a large number of selective recognition sites for epitope (9-mer peptides) of viscumin (ML1 protein) in its standard media. The molecular imprinted polymer was implemented as tailor-made polymer materials using micro-contact concept by UV in-situ polymerization in the detection of epitope from buffer samples. The most stable complex was established with the molar ratio of template to functional monomer equal to 1:4. Binding characteristics of polymers were estimated with the schatchard plot as well as stern-volmer (S–V) for analyzing quenching data. Consequently, the promising results of present work based on the high affinity of MIP prepared on modified glass to epitope as well as its good LOD, LOQ, recovery and linear range of detection - especially in complex media such as plasma and urine as well as tolerating a 12 order of magnitude of competent protein with the maximum homology with analyte (viscumin)- provides a suitable basis for the development of applications of MIP nano-biosensors in the separation and detection of 9-mer epitope as a representative of viscumin in different media.

Declaration of competing interest

The authors declare that they have no known competing financial interests or personal relationships that could have appeared to influence the work reported in this paper.

CRediT authorship contribution statement

S. Nasirahmadi: Conceptualization, Methodology, Software, Writing - original draft, Data curation, Visualization, Formal analysis, Writing - review & editing, Validation. **B. Akbari-Adergani:** Methodology, Data curation, Supervision, Validation, Resources, Project administration.

Acknowledgements

The food and drug control reference laboratories due his fully laboratory facilities support in this work is acknowledged.

Abbreviations

ML1	mistletoe lectin 1(viscumin)
EGDMA	ethylene glycol dimethacrylate
MAA	Methacrylic acid
MIP	Molecularly imprinted polymer
NIP	non-imprinted polymer

References

[1] R. Vago, Ribosome inactivating proteins: exploiting plant weapons to fight human cancer, J. Genet. Syndr. Gene Ther. 6 (2015) 272, https://doi.org/10.4172/2157-7412.1000272.
[2] Y. Sun, F. Sun, J. Li, M. Wu, X. Fan, Y. Meng, Y. Meng, Mono-PEGylation of alpha-MMC and MAP30 from momordica charantia L.: production, identification and anti-tumor activity, Molecules 21 (2016) 1457, https://doi.org/10.3390/molecules21111457.
[3] P. Jiménez, P. Cabrero, D. Cordoba-Diaz, M. Cordoba-Diaz, M. Garrosa, T. Girbés, Lectin digestibility and stability of elderberry antioxidants to heat treatment in vitro, Molecules 22 (2017) 95, https://doi.org/10.3390/molecules22010095.
[4] Y. Endo, K. Tsurugi, RNA N-glycosidase activity of ricin A-chain. Mechanism of action of the toxic lectin ricin on eukaryotic ribosomes, J. Biol. Chem. 262 (17) (1987) 8128–8130.
[5] S.W. park, R. Vepachedu, N. Sharma, J.M. Vivanco, Ribosome inactivating proteins in plant biology, Planta 219 (2004) 1093–1096.
[6] J.M. Lord, R.A. Spooner, Ricin trafficking in plant and mammalian cells, Toxins (Basel) 3 (7) (2011) 787–801, https://doi.org/10.3390/toxins3070787.
[7] R.A. Spooner, J.M. Lord, Ricin trafficking in cells, Toxins (Basel) 7 (1) (2015) 49–65, https://doi.org/10.3390/toxins7010049, 9.
[8] M. de Virgilio, A. Lombardi, R. Caliandro, M.S. Fabbrini, Ribosome-inactivating proteins: from plant defense to tumor attack, Toxins (Basel) 2 (2010) 2699–2737, https://doi.org/10.3390/toxins2112699.
[9] R. Vago, C.J. Marsden, J.M. Lord, R. Ippoliti, D.J. Flavell, S.U. Flavell, A. Ceriotti, M.S. Fabbrini, Saporin and ricin A chain follow different intracellular routes to enter the cytosol of intoxicated cells, FEBS J. 272 (2005) 4983–4995, https://doi.org/10.1111/j.1742-4658.2005.04908.x.
[10] L. Polito, M. Bortolott, iM. Pedrazzi, D. Mercatelli, M.G. Battelli, i A. Bolognes, Apoptosis and necroptosis induced by stenodactylin in neuroblastoma cells can be completely prevented through caspase inhibition plus catalase or necrostatin-1, Phytomedicine 23 (1) (2016) 32–41.
[11] L. Barbieri, M. Ciani, T. Girbes, W.Y. Liu, E.J. Van Damme, W.J. Peumans, F. Stripe, Enzymatic activity of toxic and non-toxic type 2 ribosome-inactivating proteins, FEBS Lett. 563 (2004) 219–222, https://doi.org/10.1016/S0014-5793(04)00286-8.
[12] T. Girbes, L. Citores, R. Iglesias, J.M. Ferreras, R. Munoz, M.A. Rojo, F.J. Arias, J.R. Garcia, E. Mendez, M. Calonge, Ebulin 1, a nontoxic novel type 2 ribosome-inactivating protein from *Sambucus ebulus* L. leaves, J. Biol. Chem. 268 (1993) 18195–18199.
[13] S. Reinbothe, C. Reinbothe, J. Lehmann, W. Becker, K. Apel, r.B. Parthie, JIP60, a methyl jasmonate-induced ribosome-inactivating protein involved in plant stress reactions, Proc. Natl. Acad. Sci 91 (15) (1994) 7012–7016, https://doi.org/10.1073/pnas.91.15.7012.
[14] J.K. Kim, X. Duan, R. Wu, S.J. Seok, R.S. Boston, I.C. Jang, B.H. Nahm, Molecular and genetic analysis of transgenic rice plants expressing the maize ribosome-inactivating protein b-32 gene and the herbicide resistance bar gene, Mol. Breed. 5 (2) (1999) 85–94.

[15] J. Mundy, R. Leah, R. Boston, Y. Endo, F. Stirpe, Genes encoding ribosome-inactivating proteins, Plant Mol. Biol. Rep. 12 (2) (1994) S60–S62.
[16] R. Zhang, Y. Xu, Y. Zhang, H.S. Kim, A. Sharma, J. Gao, G. Yang, J.S. Kim, Y. Sun, Rational design of a multifunctional molecular dye for dual-modal NIR-II/photoacoustic imaging and photothermal therapy, Chem. Sci. 10 (2019) 8348–8353, https://doi.org/10.1039/C9SC03504D.
[17] X. Lu, Y. Zhan, Q. Ouyang, S. Bai, H. Chen, Y. Yu, Y. Zheng, Y. Sun, H. Li, Fabrication of a tyrosine-responsive liquid quantum dots based biosensor through host–guest chemistry, Anal. Chem. 91 (20) (2019) 13285–13289, https://doi.org/10.1021/acs.analchem.9b04034.
[18] Y. Sun, F. Ding, Z. Zhou, C. Li, M. Pu, Y. Xu, Y. Zhan, X. Lu, H. Li, G. Yang, Y. Sun, P.J. Stang, Rhomboidal Pt(II) metallacycle-based NIR-II theranostic nanoprobe for tumor diagnosis and image-guided therapy, PNAS 116 (6) (2019) 1968–1973, https://doi.org/10.1073/pnas.1817021116.
[19] Y. Sun, S. Chen, X. Chen, Y. Xu, S. Zhang, Q. Ouyang, G. Yang, H. Li, A highly selective and recyclable NO-responsive nanochannel based on a spiroring opening–closing reaction strategy, Nat. Commun. 10 (2019) **1**323, https://doi.org/10.1038/s41467-019-09163-4.
[20] B. Ingrid, A.T. Scherrine, H. Akhtar, M. Jean-Louis, New biorecognition molecules in biosensors for the detection of toxins, Biosens. Bioelectron. 87 (2017) 285–298, https://doi.org/10.1016/j.bios.2016.06.083.
[21] R. Ranjana, E.N. Esimbekovaa, V.A. Kratasyuk, Rapid biosensing tools for cancer biomarkers, Biosens. Bioelectron. 87 (2017) 918–930, https://doi.org/10.1016/j.bios.2016.09.061.
[22] P.U. Sruthi, M.Sh Anand, D.G. Banshi, A contemporary approach for design and characterization of fiber-optic-cortisol sensor tailoring LMR and ZnO/PPY molecularly imprinted film, Biosens. Bioelectron. 87 (2017) 178–186.
[23] E. Komarova, M. Aldissi, A. Bogomolova, Design of molecularly imprinted conducting polymer protein-sensing films via substrate–dopant binding, Analyst 140 (4) (2015) 1099–1106, https://doi.org/10.1039/C4AN01965B.
[24] G. Ertürk, D. Berillo, M. Hedström, B. Mattiasson, Microcontact-BSA imprinted capacitive biosensor for real-time, sensitive and selective detection of BSA, Biotechnol. Rep 3 (2014) 65–72, https://doi.org/10.1016/j.btre.2014.06.006.
[25] S. Pradhan, M. Boopathi, O. Kumar, A. Baghel, P. Pandey, T.H. Mahato, B. Singh, R. Vijayaraghavan, Molecularly imprinted nanopatterns for the recognition of biological warfare agent ricin, Biosens. Bioelectron. 25 (3) (2009) 592–598, https://doi.org/10.1016/j.bios.2009.03.041.
[26] F. Breton, R. Delepee, D. Jegourel, D. Deville-Bonne, L.A. Agrofoglio, Selective adenosine-5′-monophosphate uptake by water-compatible molecularly imprinted polymer, Anal. Chim. Acta 616 (2008) 222–229, https://doi.org/10.1016/j.aca.2008.04.025.
[27] A. Rachkov, N. Minour, Recognition of oxytocin and oxytocin-related peptides in aqueous media using a molecularly imprinted polymer synthesized by the epitope approach, J. Chromatogr. A 889 (2000) 111–118, https://doi.org/10.1016/S0021-9673(00)00568-9.
[28] L. Mei, G. Somesfalean, S. Svanberg, Optical characterization of micro-porous ceramics using tunable diode laser, Proceedings (2013) 8570, https://doi.org/10.1117/12.2005311. Frontiers in Biological Detection: From Nanosensors to Systems V, 85700O.
[29] Y. Yang, Q. Tang, C. Gong, X. Ma, J. Peng, M.H. Lam, Ultrasensitive detection of bisphenol A in aqueous media using photoresponsive surface molecular imprinting polymer microspheres, New J. Chem. 38 (2014) 1780–1788, https://doi.org/10.1039/C3NJ01598J.
[30] A.N. Karaseva, B. Pluhar, A.E. Beliaeva, N.T. Ermolaeva, B. Mizaikoff, Synthesis and application of molecularly imprinted polymers for trypsin piezoelectric sensors, Sens. Actuators, B 280 (2019) 272–279, https://doi.org/10.1016/j.snb.2018.10.022.
[31] Z. Sun, rW. Schüssle, M. Sengl, R. Niessner, D. Knopp, Selective trace analysis of diclofenac in surface and wastewater samples using solid-phase extraction with a new molecularly imprinted polymer, Anal. Chim. Acta 620 (2008) 73–81, https://doi.org/10.1016/j.aca.2008.05.020.
[32] Y.J. Hu, Y. Liu, J.B. Wang, X.H. Xiao, S.S. Qu, Study of the interaction between monoammonium glycyrrhizinate and bovine serum albumin, J. Pharm. Biomed. Anal 36 (2004) 915–919, https://doi.org/10.1016/j.jpba.2004.08.021.
[33] S.K. Ghosh, A. Pal, S. Kundu, S. Nath, T. Pal, Fluorescence quenching of 1-methylaminopyrene near gold nanoparticles: size regime dependence of the small metallic particles, Chem. Phys. Lett. 395 (2004) 366–372, https://doi.org/10.1016/j.cplett.2004.08.016.
[34] D. Zhao, T.M. Swager, Sensory responses in solution vs solid state: a fluorescence quenching study of poly (Iptycenebutadiynylene)s, Macromolecules 38 (22) (2005) 9377–9384, https://doi.org/10.1021/ma051584y.
[35] X. Zhang, S. Yang, R. Jiang, L.Q. Sun, S.P. Pang, A.Q. Luo, Fluorescent molecularly imprinted membranes as biosensor for the detection of target protein, Sens. Actuators, B 254 (2018) 1078–1086, https://doi.org/10.1016/j.snb.2017.07.205.
[36] H. Elmizadeh, F. Faridbod, M. Soleimani, M. Ganjali, G. Rezanejade Bardajee, Fluorescent apta-nanobiosensors for fast and sensitive detection of digoxinin biologicalfluids using rGQDs: comparison of two approaches forimmobilization of aptamer, Sens. Actuators, B 302 (2020) 127133, https://doi.org/10.1016/j.snb.2019.127133.
[37] G. den Boef, A. Hulanicki, Recommendations for the Usage of Selective, Selectivity and Related Terms in Analytical Chemistry, published online 2009.01.01. DOI: https://doi.org/10.1351/pac198855030553.
[38] S. Pradhan, M. Boopathi, O. Kumar, A. Baghel, P. Pandey, T.H. Mahato, B. Singh, R. Vijayaraghavan, Molecularly imprinted nanopatterns for the recognition of biological warfare agent ricin, Biosens. Bioelectron. 25 (3) (2009) 592–598, https://doi.org/10.1016/j.bios.2009.03.041.
[39] E. Komarova, M. Aldissi, A. Bogomolova, Design of molecularly imprinted conducting polymer protein-sensing films via substrate-dopant binding, Analyst 140 (4) (2015) 1099–1106, https://doi.org/10.1039/c4an01965b.
[40] P. Ravichandiran, S. Allur Subramaniyan, A. Paulraj Bella, P. Merlin Johnson, A.R. Kim, K. Seob Shim, D. Jin Yoo, Simple fluorescence turn-on chemosensor for selective detection of Ba2+ ion and its live cell imaging, Anal. Chem. 91 (15) (2019) 10095–10101, https://doi.org/10.1021/acs.analchem.9b02057.
[41] P. Ravichandiran, A. Boguszewska-Czubara, M. Masłyk, A. Paulraj Bella, S. Allur Subramaniyan, P. Merlin Johnson, K. Seob Shim, H. Gyu Kim, D. Jin Yoo, Naphthoquinone-based colorimetric and fluorometric dual-channel chemosensor for the detection of Fe2+ ion and its application in bio-imaging of live cells and zebrafish, ACS Sustain. Chem. Eng. 7 (20) (2019) 17210–17219, https://doi.org/10.1021/acssuschemeng.9b03822.
[42] P. Ravichandiran, A. Boguszewska-Czubara, M. Masłyk, A. PaulrajBella, P. MerlinJohnson, S. AllurSubramaniyan, K. SeobShim, D. JinYoo, A phenoxazine-based fluorescent chemosensor for dual channel detection of Cd2+ and CN− ions and its application to bio-imaging in live cells and zebrafish, Dyes Pigments 172 (2020) 107828, https://doi.org/10.1016/j.dyepig.2019.107828.